Investigation and optimization of interface reactivity between $Ce_{0.9}Gd_{0.1}O_{1.95}$ and $Zr_{0.89}Sc_{0.1}Ce_{0.01}O_{2-\delta}$ for high performance intermediate temperature-solid oxide fuel cells

Zhenwei Wang*, Shin-ichi Hashimoto[1], Masashi Mori

Materials Science Research Laboratory, Central Research Institute of Electric Power Industry, 2-6-1 Nagasaka, Yokosuka, Kanagawa 240-0196, Japan

ARTICLE INFO

ABSTRACT

The effects of cobalt addition on the sintering, thermal, and electrical properties of $Ce_{0.9}Gd_{0.1}O_{1.95}$ (GDC) and $Zr_{0.89}Sc_{0.1}Ce_{0.01}O_{2-\delta}$ (ScSZ) were investigated. A small addition of cobalt oxide remarkably enhanced the sinterability of GDC, especially for GDC powder with a specific surface area of $40\,m^2\,g^{-1}$, which was synthesized via a citrate method. Relative densities of approximately 95% can be achieved for GDC pellet samples using 2 mol% Co dopant and sintering at 1100 °C for 10 h. The thermal expansion and electrical conductivity of 2 mol% Co-doped GDC were comparable to those of the non-doped sample. The thermal expansion of ScSZ with various amounts of Co addition was linear in both oxidizing and reducing atmospheres. The electrical conductivity of Co-doped ScSZ decreased with increasing Co content; however, this decrease was not dramatic. These results suggest that the addition of cobalt oxide is a promising method for obtaining GDC buffer layers that are sinterable at low temperatures for use in intermediate temperature-solid oxide fuel cells.

© 2009 Elsevier B.V. All rights reserved.

1. Introduction

Solid oxide fuel cells (SOFCs) have attracted increasing attention in recent years because of their high energy conversion efficiency, low NO_x emissions and flexible fuel requirements. The development of intermediate temperature SOFCs operated at 500–650 °C is very important due to the possibility that low-cost metallic alloys may be used in the SOFCs. Compared to an electrolyte-supported design, an anode-supported SOFC is more suitable for lower temperature operation because of its smaller ohmic loss of electrolyte and better interface contact between the electrolyte and electrodes [1–4].

Our group has successfully fabricated anode-supported microtubular cells with a configuration of $La_{0.6}Sr_{0.4}Co_{0.2}Fe_{0.8}O_{3-\delta}$ (LSCF)–$Ce_{0.8}Gd_{0.2}O_{1.9}$ (GDC) cathode/GDC buffer layer/ $Zr_{0.89}Sc_{0.1}Ce_{0.01}O_{1.95}$ (ScSZ) electrolyte/Ni–ScSZ anode [5–8]. In this research, the performance of the individual cells was high, but a large voltage drop in the low current density region was problematic. To clarify the causes of this drop, transmission electron microscopy (TEM) with energy dispersive X-ray (EDX) analysis of the interface between the GDC buffer layer and the ScSZ electrolyte was performed after the cell was cross-sectioned using a focused ion beam (FIB).

Fig. 1a shows the TEM image, and Fig. 1b shows the results of the EDX analysis. Many pores were observed in the GDC buffer layer. Moreover, the diffusion of Zr from the ScSZ electrolyte into the GDC layer was confirmed, although Zr did not seem to reach the LSCF–GDC cathode. It has been reported that Zr diffusion and pore formation lower oxide-ionic conductivity [9–11]. In the fabrication of our cells, after the GDC buffer layer was dip-coated onto a dense ScSZ electrolyte that had been fired at 1400 °C for 6 h, the layer was sintered at 1200 °C for 4 h. The high firing temperature of GDC probably caused the observed reaction between GDC and ScSZ. These findings make it necessary to develop a GDC buffer layer film that can be sintered at lower temperatures (<1200 °C) and coated onto a ScSZ electrolyte with better adhesion and higher densification.

Many reports have shown that the addition of cobalt oxides as a sintering aid enhances the sintering characteristics of GDC powder [12–14]. In addition, Yamahara et al. [15] showed that cobalt infiltration in a La_2O_3-based perovskite cathode decreased the effective charge transfer resistance, and thus improved the cell performance. Based on these results, cobalt oxide may be a good candidate as a sintering aid for the GDC buffer layer. However, Co easily vaporizes and tends to form reaction products with low melting points [16,17]. There is a possibility that CoO, which is contained in the Co-doped GDC buffer layer, may diffuse into the ScSZ electrolyte during the sintering process. Therefore, it is necessary to examine the thermal expansivity and electrical conductivity of ScSZ doped with Co.

* Corresponding author. Tel.: +81 46 856 2121; fax: +81 46 856 5571.
E-mail address: kooichi_cn@hotmail.com (Z. Wang).
[1] Present address: Tohoku University, Graduate School of Engineering, Department of Materials Science.
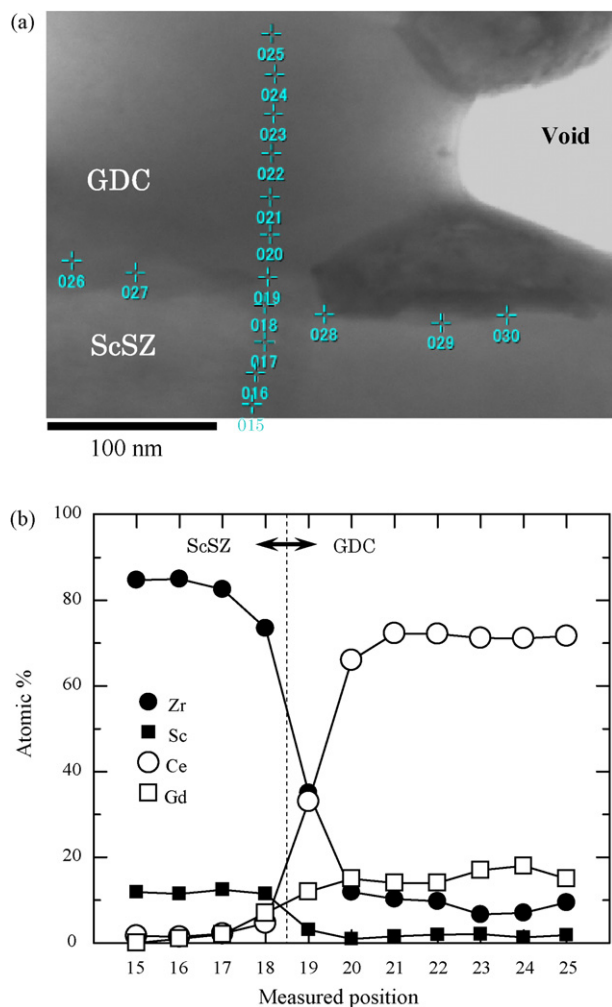
Fig. 1. (a) TEM image for cross-section of SOFC and the EDX analysis points. (b) Quantitative analysis of the elements by EDX as a function of the location.

This study aims to study the effect of Co dopant on the sintering characteristics, thermal expansion behavior and electrical conductivity of GDC. Furthermore, the thermal and electrical properties of Co-doped ScSZ were measured in order to clarify the potential effects of Co on ScSZ.

2. Experimental

The $Ce_{0.9}Gd_{0.1}O_{1.95}$ (10 mol% gadolinium-doped ceria, GDC) powders used in this study were synthesized in two different ways: the conventional citrate method or a coprecipitation method [18–20]. Two kinds of GDC powder were synthesized by the citrate method. The powders, GDCA10 and GDCA40, had specific surface areas of 10 and 40 $m^2 g^{-1}$, respectively. The GDC powder synthesized by the coprecipitation method, GDCB40, had a specific surface area of 40 $m^2 g^{-1}$.

Each GDC powder was mixed with CoO (High Purity Chem., Japan) via a solid-state technique. The molar ratios of GDC to Co were 100:0, 99:1, 98:2 and 97:3. In order to measure sintering behavior, the prepared powder mixtures were pressed into tablets 20 mm in diameter and 2 mm in thickness by uniaxial dry pressing at 23 MPa. The compacted GDC tablets used to examine sintering behavior were then sintered in air at temperatures of 900–1100 °C with a heating rate of 200 °C h^{-1}. The densities of the sintered tablets were determined from the size and weight of tablets. Relative densities were derived using the observed and theoretical
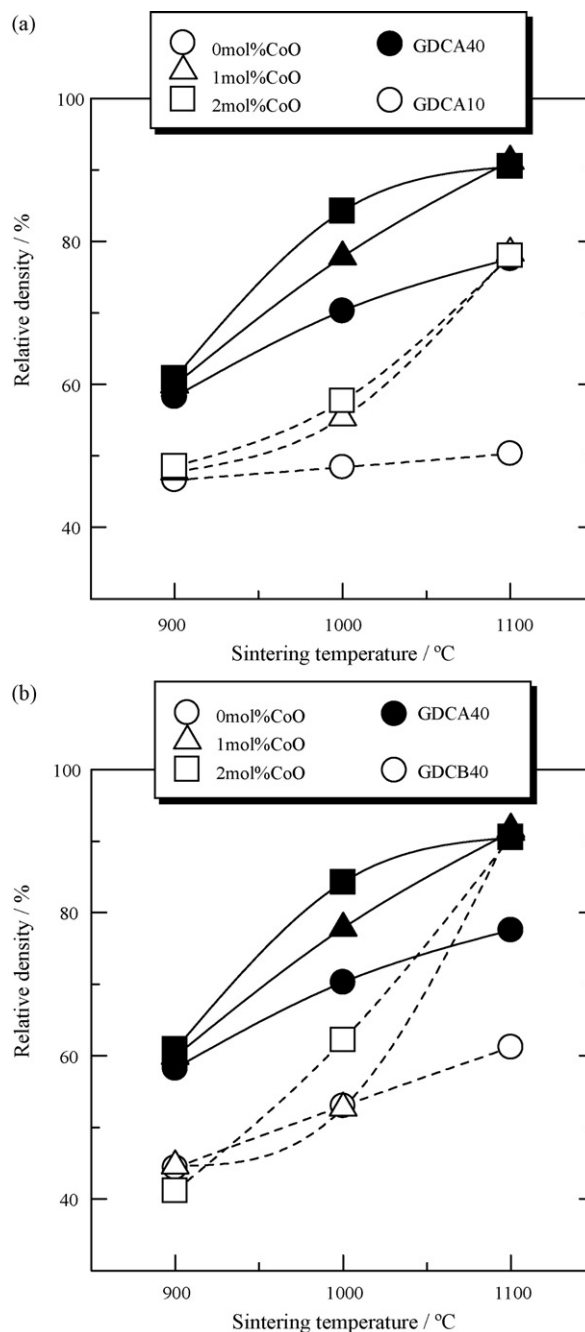

Fig. 2. Relative densities of Co-doped GDC without holding time, as a function of sintering temperature. (a) Comparison of GDCA10 and GDCA40. (b) Comparison of GDCA40 and GDCB40. A: citrate method, B: coprecipitation method, 10: 10 $m^2 g^{-1}$, 40: 40 $m^2 g^{-1}$.

densities. The theoretical densities were calculated from the lattice parameters and unit formula based on powder X-ray diffraction (XRD, Rigaku, 18 kW, ultraX 18TTR2-300, Japan). XRD was also used to analyze the crystal structures of all samples. The scanning rate was 0.02 s^{-1}.

The conductivities of the samples were examined by an AC impedance method at temperatures of 450–850 °C in both air and in a reducing atmosphere (3% humidified 33% H_2 in N_2). The Pt electrodes were attached to the tablets using Pt paste and sintered at 900 °C for 1 h in air. The AC impedance was measured between 0.1 and 100 MHz with a frequency response analyzer and a potentiostat (Solartron 1260 and 1286, respectively). An applied potential of 10 mV was used.
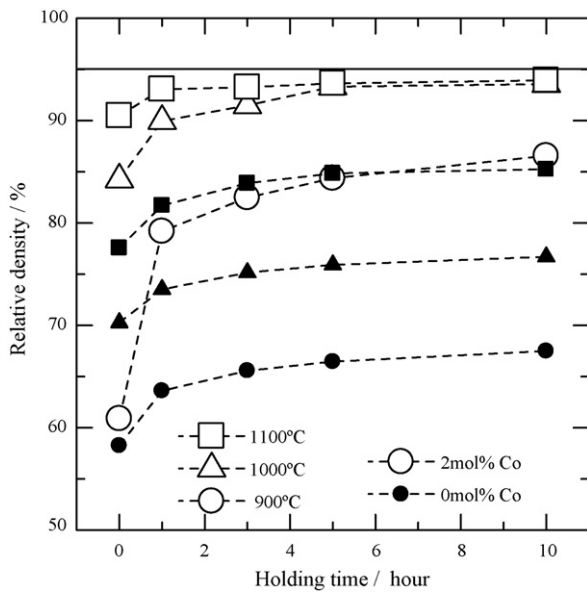
Fig. 3. Relatively densities of 0 mol% (closed symbols) and 2 mol% (open symbols) Co-doped GDC as a function of sintering temperature. (GDC powder: citrate method, 40 m² g⁻¹.)

To investigate the thermal expansion behavior, dense rectangular samples were prepared with dimensions of approximately 5 mm × 5 mm × 16 mm. The thermal expansion was measured in air and in 10 °C humidified H_2 from 50 to 900 °C using a Mac Science TG–DTA 5000S system. The rate of heating and cooling was 2 °C min⁻¹, and a rod of Al_2O_3 was used as a reference.

With the exception of the sintering temperatures, the preparation processes of pure and Co-doped ScSZ (Daiichi Kigenso Kagaku Kogyo Co. Ltd., Japan) were the same as those for GDC. ScSZ samples used for XRD analysis were sintered at 1100 °C, and the samples used to measure electrical conductivity and thermal expansion were sintered at 1400 °C.

3. Results and discussion

3.1. Sintering characteristics of Co-doped GDC

The effect of the specific surface area on the sintering characteristics of Co-doped GDC was examined. Fig. 2 shows the relative densities of non-doped as well as 1 and 2 mol% Co-doped GDC as a function of firing temperature. The holding time at the highest temperature was zero. At sintering temperatures less than 900 °C, Co doping had almost no effect enhancing the sintering characteristics. However, Co doping obviously sped the densification of GDC at temperatures greater than 1000 °C. The increase in densification was the same for both 1 and 2 mol% Co-doped samples. The effect was especially remarkable at 1100 °C. For all Co-doped samples, the sintering characteristics of GDCA40 were higher than those of GDCA10, as shown in Fig. 2a.

The effects of Co doping on the sintering behavior of the GDC powders prepared by different synthetic methods were also compared. Fig. 2b shows the relative densities of pure and Co-doped GDC as a function of firing temperature. The holding time was zero. At a sintering temperature of 1100 °C, the relatively densities of samples with less than 1 mol% doping reached almost 90% for GDC powders prepared by both synthetic methods. However, at temperatures less than 1100 °C, GDCA40 had more favorable sintering characteristics than GDCB40. This result is likely due to the different powder shapes and particle size distributions of the two powders. TEM micrographs reveal that GDCA40 is composed of dispersed,
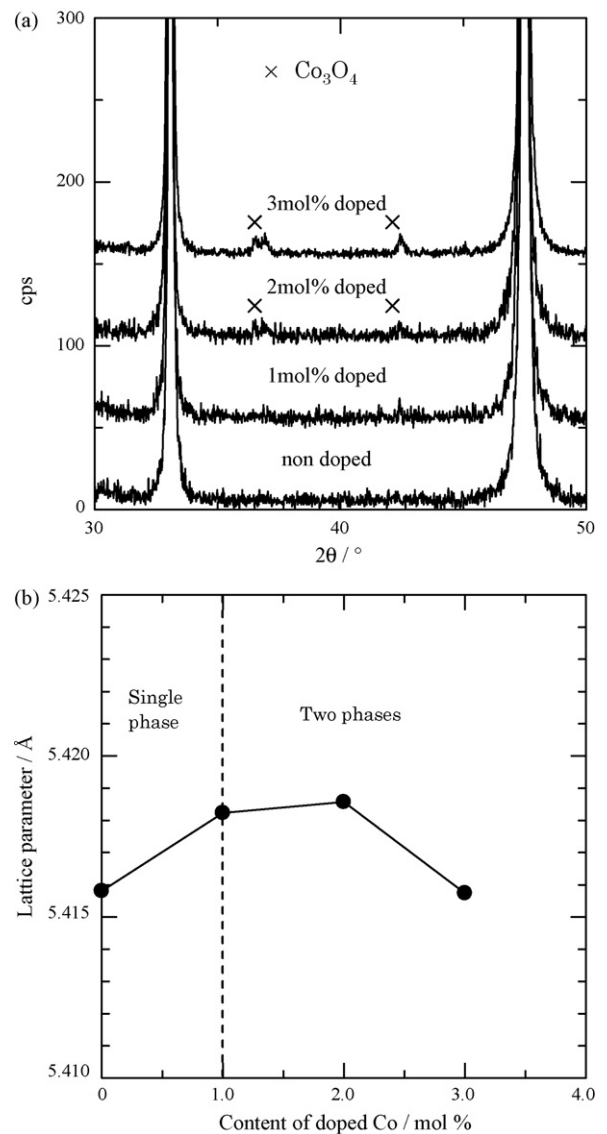

Fig. 4. (a) X-ray diffraction patterns and (b) lattice parameters of Co-doped GDC. (GDC: citrate method, 40 m² g⁻¹. Samples were heated at 1100 °C for 10 h.)

spherical particles, whereas GDCB40 contains particle agglomerations [18]. GDCB40 seems to be more porous. Thus, pores formed easily during sintering and inhibited the densification. Based on these results, the GDCA40 starting material will be the focus of the following discussion of Co-doped GDC.

The effect on densification of sintering holding time at the highest sintering temperature was also investigated. Fig. 3 shows the effect of Co addition on the density of sintered GDC as a function of holding time at 900, 1000 and 1100 °C; the closed and open symbols represent the data for pure GDC and for 2 mol% Co-doped samples, respectively. The relative densities increased rapidly after sintering for about 4 h. This was then followed by a slow approach to saturation. Usually, this behavior is observed for solid-state sintering mechanisms. For pure GDC, a relative density of only 85% was obtained after sintering at 1100 °C for 10 h. On the other hand, in the case of the 2 mol% Co-doped sample, the relative density reached nearly 95%. It should be pointed out that with 2 mol% Co addition, the relative density of GDC sintered at 1000 °C was almost the same as that of the sample sintered at 1100 °C after 5 h. This suggests a low firing temperature below 1100 °C may be used to obtain denser GDC membranes via the addition of 2 mol% Co as a sintering agent.
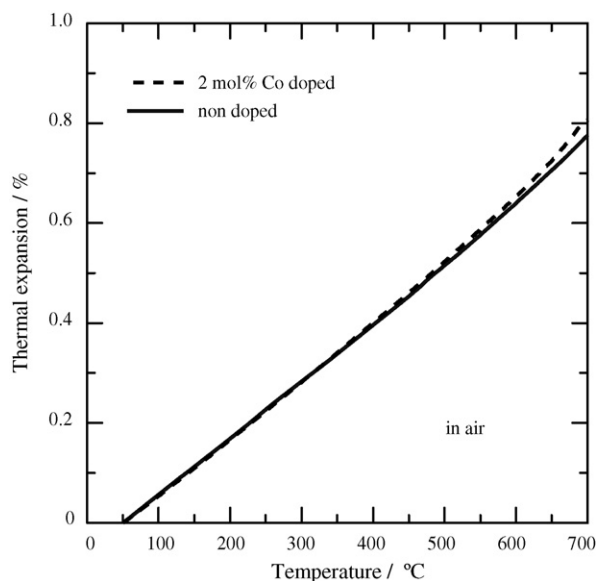
Fig. 5. Thermal expansion behaviors of non-doped GDC and 2 mol% Co-doped GDC in air. GDC powder: citrate method, 40 m² g⁻¹. Samples were heated at 1100 °C for 10 h.

Fig. 6. Electrical conductivities of non-doped GDC and 2 mol% Co-doped GDC in air. (GDC powder: citrate method, 40 m² g⁻¹. Samples were heated at 1100 °C for 10 h.)

3.2. X-ray diffraction of Co-doped GDC

The X-ray diffraction patterns of 0–3 mol% Co-doped GDCA40 samples obtained after firing at 1100 °C for 10 h are shown in Fig. 4a. No peaks associated with Co_3O_4 were observed in the 1 mol% Co-doped GDC. With increasing amounts of Co additions, the Co_3O_4 peaks increased.

Fig. 4b shows the lattice parameters calculated from the data in Fig. 4a. It is apparent that the lattice parameters of doped GDC increased with increasing Co content up to 2 mol% and then decreased. Because a second phase was observed at approximately 2 mol%, the solubility limit of Co should be less than 2 mol%. The decrease in lattice parameter for 3 mol% Co-doped GDC might be related to the decrease in the Gd element concentration in GDC [21], indicating the possibility of a reaction between CoO and Gd, although no peaks of products such as $GdCoO_3$ were detected by XRD.

3.3. Thermal expansion behaviors and electrical conductivities of Co-doped GDC

Fig. 5 shows the thermal expansion behavior of the 2 mol% Co-doped GDC sample in air. For comparison, the non-doped GDC sample is also shown. The thermal expansion coefficient (TEC) in the temperature range between 50 and 650 °C was $12 \times 10^{-6} \, °C^{-1}$, which is in accordance with the typical TEC values reported in the literature for GDC [22,23]. It was observed that the Co-doped GDC m expanded at temperatures around 600 °C; however, this expansion was small. This is postulated to be related to changes in the valence and spin condition of the cobalt ion [24].

The electrical conductivities of the GDC samples are shown in Fig. 6. Although it is known that the reproducibility of conductivity data for CeO_2-based oxides is not high [25–28], the conductivity of pure GDC in this study was comparable to the data reported by Hohnke [26]. As can be seen in Fig. 6, the Co-doped GDC showed a higher conductivity than the non-doped sample. This improvement in the electrical conductivity of GDC by Co addition is possibly due to (i) a reduction in the lattice strain of GDC by Co and (ii) the formation of a Co-rich grain boundary layer.

Lewis et al. [29] found that due to a relaxation effect, the activation energy (Ea) for the conductivity of Co-doped GDC was lower
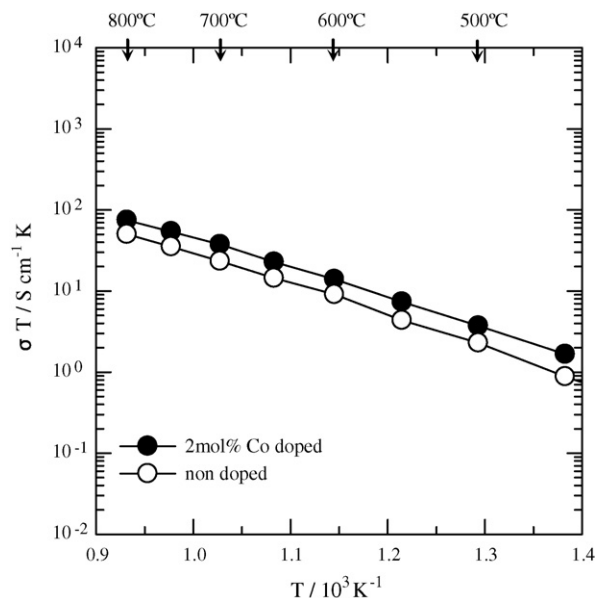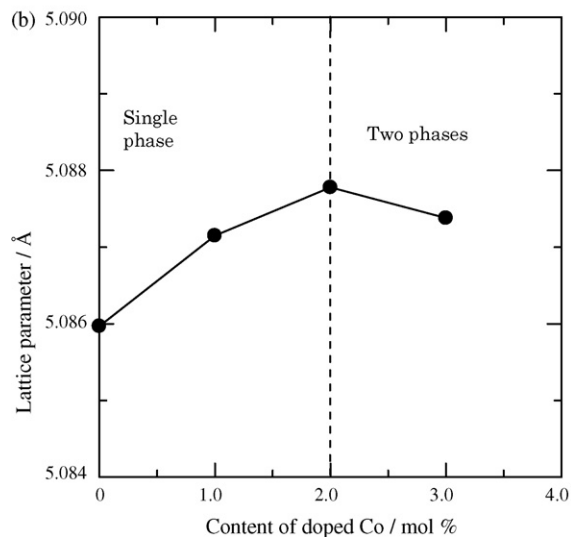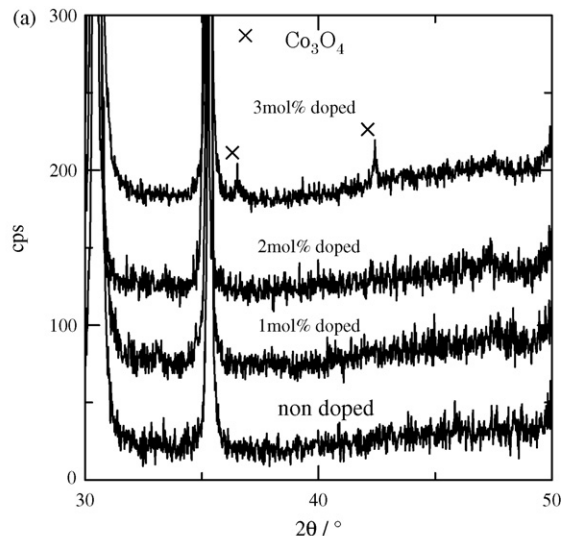

Fig. 7. (a) X-ray diffraction patterns, (b) lattice parameters of Co-doped ScSZ. (Samples were heated at 1100 °C for 10 h.)

that that of the pure material. A similar trend was also observed in this study. The Ea for non-doped GDC was 0.86 eV, while the Ea for 2 mol% Co-doped GDC was 0.74 eV. In our samples, such a "relaxation effect" might have also occurred, and thus enhanced the electrical conductivity of GDC. On the other hand, Gauckler and coworkers [30–32] reported that in Co-doped GDC that had been sintered at temperatures higher than 900 °C, excess cobalt easily agglomerated in the GDC grain boundary, and the electronic conductivity along the percolating Co-rich grain boundary layer short-circuited the ionic conductivity of the GDC grains. As shown in Fig. 4, a Co_3O_4 peak was detected in the 2 mol% Co-doped GDC sample. This indicates the possibility that a Co-rich grain boundary layer formed, and thus might have improved the electrical conductivity.

3.4. X-ray diffraction of Co-doped ScSZ

As previously reported in this study, the GDC buffer layer may be sinterable at a lower temperature with the use of 2 mol% Co dopant. It is known that CoO easily vaporizes at temperatures as low as 900 °C [12]. Thus, there is the possibility of diffusion of Co from the GDC layer into the ScSZ electrolyte.

Fig. 7a shows the X-ray diffraction patterns of Co-doped ScSZ after firing at 1100 °C for 10 h. A peak attributable to Co_3O_4 was detected in the sample doped with 3 mol% Co; no peaks for any other second phases were observed. Furthermore, no change in the cubic structure of the doped ScSZ was observed. Fig. 7b shows the calculated lattice parameters of the doped ScSZ using the data from Fig. 7a. It can be seen that the value of the lattice parameter slightly increased as the amount of Co dopant increased to 2 mol%, and then slightly decreased. From these data, the solubility limit of Co in ScSZ seems to be less than or equal to 2 mol%.

3.5. Thermal expansion behaviors and electrical conductivities of Co-doped ScSZ

Fig. 8 shows the thermal expansion curves of Co-doped ScSZ in the temperature range of 50–900 °C in air and in a H_2 atmosphere. TECs calculated from 50 to 650 °C (the operating temperature of our anode-supported SOFCs using ScSZ electrolytes [5–8]) are sum-

Table 1
Thermal expansion coefficients (TECs) (50–650 °C) of pure and Co-doped ScSZ in air, and in 10 °C humidified H_2.

ScSZ samples	TEC ($\times 10^{-6}$ °C^{-1}) 50–650 °C	
	In air	In H_2
Pure ScSZ	9.8	9.3
1 mol% Co doped	9.4	9.2
2 mol% Co doped	9.6	9.5
3 mol% Co doped	9.6	9.3

marized in Table 1. The TECs of ScSZ samples with varying Co content are almost identical in air and in the reducing atmosphere.

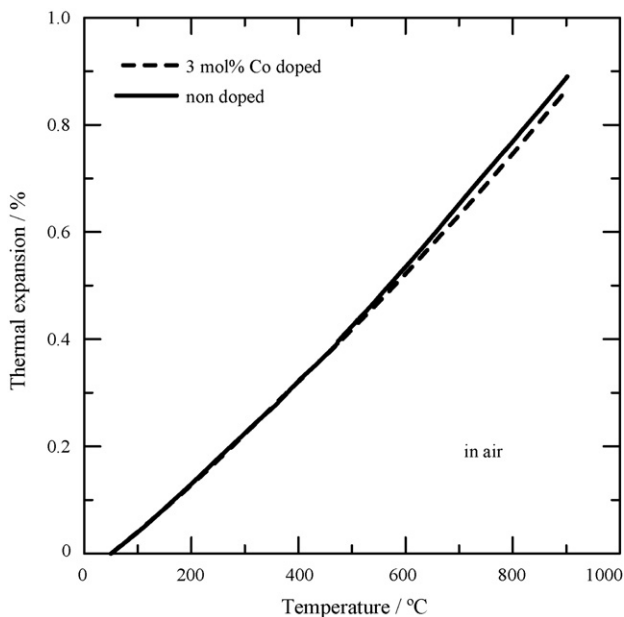Fig. 9a shows the Arrhenius plots of Co-doped ScSZ in air. The electrical conductivities as a function of the Co concentration in air and in the reducing atmosphere are shown in Fig. 9b. It was observed that the conductivity of the pure ScSZ was highest. The conductivities of Co-doped ScSZ decreased with increasing Co content. However, the difference in conductivity between pure and

Fig. 8. Thermal expansion behaviors of Co-doped ScSZ in air, and in 10 °C humidified H_2. (Samples were heated at 1400 °C for 4 h.)
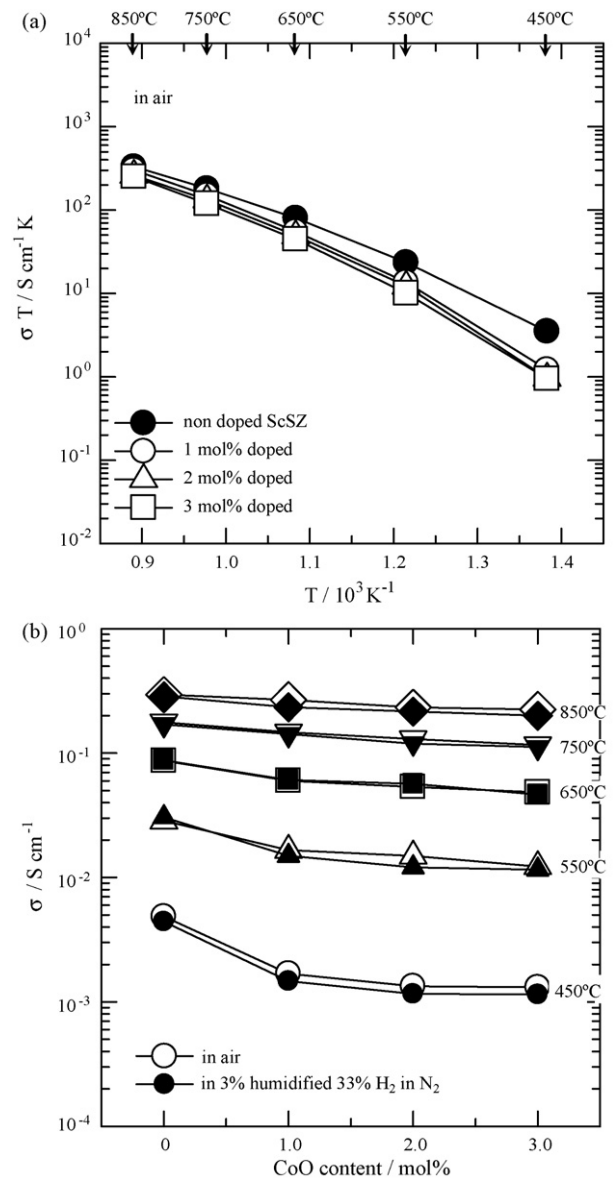

Fig. 9. Electrical conductivities of Co-doped ScSZ as a function of (a) temperature and (b) Co content. (Samples were heated at 1400 °C for 4 h.)

Table 2
Electrical conductivities of pure and Co-doped ScSZ at 650 °C, in air, and in 3% humidified 33% H_2 in N_2.

ScSZ samples	Electric conductivities (S cm^{-1}) at 650 °C	
	In air	In H_2
Pure ScSZ	0.087	0.087
1 mol% Co doped	0.060	0.061
2 mol% Co doped	0.053	0.056
3 mol% Co doped	0.048	0.046

Co-doped ScSZ decreased with increasing temperature. The calculated Ea was 0.72 eV for pure ScSZ, and 0.88, 0.90, 0.90 for the 1, 2, 3 mol% Co-doped ScSZ, respectively. The highest Ea for a pure ScSZ comparing to those for Co-doped samples, indicated that the ion immigration was easier in the non-doped ScSZ.

Table 2 summarizes the electric conductivity of the pure and Co-doped ScSZ at the expected cell operating temperature of 650 °C. The electrical conductivity of 0.087 S cm^{-1} for a pure ScSZ was consistent with the value reported by Yamamoto et al. [33]. Although the Co addition lowered the electrical conductivity of ScSZ, it was not serious. It should also be pointed out that the conductivity in the reducing atmosphere was nearly the same as in air. The conformity of the electrical conductivities for both environments indicates that no electronic conductivity appeared. This property is important to ensure the open-circuit voltage and the efficiency of the cell.

4. Conclusion

The relative densities, thermal expansion behaviors and electrical conductivities of $Ce_{0.9}Gd_{0.1}O_{1.95}$ and $Zr_{0.89}Sc_{0.1}Ce_{0.01}O_{1.95}$ using cobalt as a sintering aid were investigated. The effect of the Co dopant on the sintering characteristics of GDC is more remarkable for GDC powder with a larger specific surface area. The enhancement of sintering behavior by Co doping is different for GDC powders prepared by different synthetic methods. Co addition does not affect the thermal expansion behavior of GDC, while it improves the electrical conductivity. The Co dopant does not affect the thermal expansion behavior of ScSZ, whereas the conductivity has a tendency to decrease with increasing Co content. However, this effect is considered to be small at intermediate temperatures. Co doping of GDC is a promising way to lower the firing temperature of the buffer layer on ScSZ electrolytes in anode-supported SOFCs.

References

[1] F. Zhao, A.V. Virkar, J. Power Sources 141 (2005) 79.
[2] T.L. Nguyen, K. Kobayashi, T. Honda, T. Kato, Solid State Ionics 174 (2004) 163.
[3] A.V. Virkar, J. Chen, C.W. Tanner, J.W. Kim, Solid State Ionics 131 (2000) 189.
[4] A.C. Müller, D. Herbstritt, E. Ivers-Tiffée, Solid State Ionics 152 (153) (2002) 537.
[5] S. Hashimoto, H. Nishino, Y. Liu, K. Asano, K. Takei, M. Mori, Y. Funahashi, Y. Fujishiro, ECS Trans. 7 (2007) 609.
[6] S. Hashimoto, H. Nishino, Y. Liu, K. Asano, M. Mori, Y. Funahashi, Y. Fujishiro, J. Fuel Cell Sci. Technol. 5 (2008) 031208–31211.
[7] S. Hashimoto, H. Nishino, Y. Liu, K. Asano, M. Mori, Y. Funahashi, Y. Fujishiro, J. Electrochem. Soc. 155 (2008) B587.
[8] S. Hashimoto, H. Nishino, Y. Liu, K. Asano, M. Mori, Y. Funahashi, Y. Fujishiro, J. Power Sources 181 (2008) 244.
[9] K. Eguchi, N. Akasaka, H. Mitsuyasu, Y. Nonaka, Solid State Ionics 135 (2000) 589.
[10] T. Kawada, H. Yokokawa, M. Dokiya, N. Sakai, T. Horita, J. Herle, K. Sasaki, J. Electroceram. 1 (1997) 155.
[11] Z. Wang, J. Qian, S. Wang, J. Cao, T. Wen, Solid State Ionics 179 (2008) 1593.
[12] M. Mori, E. Suda, B. Pacaud, K. Murai, T. Moriga, J. Power Sources 157 (2006) 688.
[13] E. Jud, L. Gauckler, J. Electroceram. 14 (2005) 247.
[14] E. Jud, C. Huwiler, L. Gauckler, J. Ceram. Soc. Jpn. 114 (2006) 963.
[15] K. Yamahara, C.P. Jacobson, S.J. Visco, X. Zhang, L.C.D. Jonghe, Solid State Ionics 176 (2005) 275.
[16] H. Yoshida, K. Miura, J. Fujita, T. Inagaki, J. Am. Ceram. Soc. 82 (1999) 219.
[17] R. Koc, H.U. Anderson, J. Eur. Ceram. Soc. 15 (1995) 867.
[18] Y. Liu, S. Hashimoto, H. Nishino, K. Takei, M. Mori, J. Power Sources 164 (2007) 56.
[19] E. Suda, B. Pacaud, Y. Montardi, M. Mori, M. Ozawa, Y. Takeda, Electrochemistry 71 (2003) 866.
[20] E. Suda, M. Mori, K. Murai, B. Pacaud, T. Moriga, J. Ceram. Soc. Jpn. 113 (2005) 793.
[21] E. Suda, B. Pacaud, Y. Montardi, M. Mori, Y. Takeda, Trans. Mater. Res. Soc. Jpn. 29 (2004) 2317.
[22] S. Sameshima, M. Kawaminami, Y. Hirata, J. Ceram. Soc. Jpn. 110 (2002) 597.
[23] G.A. Tompsett, N.M. Sammes, O. Yamamoto, J. Am. Ceram. Soc. 80 (1997) 3181.
[24] M. Mori, Y. Hiei, T. Yamamoto, J. Am. Ceram. Soc. 84 (2001) 781.
[25] A. Trovarelli, Catalysis by Ceria and Related Materials, Imperial College Press, London, 2001, pp. 453–482, ISBN 1-86094-229-7.
[26] D.K. Hohnke, Solid State Ionics 5 (1981) 531.
[27] B.H.C. Steele, Solid State Ionics 129 (2000) 95.
[28] K. Eguchi, T. Setoguchi, T. Inoue, H. Arai, Solid State Ionics 52 (1992) 165.
[29] G.S. Lewis, A. Atkinson, B.H.C. Steele, J. Drennna, Solid State Ionics 152 (2002) 567.
[30] E. Jud, L. Gauckler, J. Electroceram. 15 (2005) 159.
[31] C. Kleinloger, L. Gauckler, J. Electroceram. 5 (2000) 231.
[32] E. Jud, Z. Zhang, W. Sigle, L. Gauckler, J. Electroceram. 16 (2006) 191.
[33] O. Yamamoto, Y. Arati, Y. Takeda, N. Imanishi, M. Mizutani, M. Kawai, Y. Nakamura, Solid State Ionics 79 (1995) 137.